Zhang *et al. Chem. Synth.* **2025**, *5*, 18
DOI: 10.20517/cs.2024.37

Chemical Synthesis

Research Article

Open Access

Continuous-flow electrooxidation for scalable biomass upgrading over copper-supported CoFe Prussian blue analogues

Bowen Zhang[1,#], Tiantian Xiao[2,#], Cejun Hu[3,*], Zhichen Liu[1], Peng Chen[1], Zhengyu Zhao[1], Duanjing Lai[3], Jinming Huang[1], Hongwei Zhang[1,*], Xiaojun Bao[1,4], Pei Yuan[1,4,*]

[1]National Engineering Research Center of Chemical Fertilizer Catalyst, College of Chemical Engineering, Fuzhou University, Fuzhou 350108, Fujian, China.
[2]Joint School of National University of Singapore and Tianjin University, International Campus of Tianjin University, Binhai New City, Fuzhou 350207, Fujian, China.
[3]College of Materials Science and Engineering, Fuzhou University, Fuzhou 350108, Fujian, China.
[4]Qingyuan Innovation Laboratory, Quanzhou 362801, Fujian, China.
[#]Authors contributed equally.

[*]**Correspondence to:** Prof. Cejun Hu, College of Materials Science and Engineering, Fuzhou University, No. 2 Wulong Jiangbei Avenue, Fuzhou 350108, Fujian, China. E-mail: cejun_hu@fzu.edu.cn; Prof. Hongwei Zhang, Prof. Pei Yuan, National Engineering Research Center of Chemical Fertilizer Catalyst, College of Chemical Engineering, No. 2 Wulong Jiangbei Avenue, Fuzhou University, Fuzhou 350108, Fujian, China. E-mail: zhanghw@fzu.edu.cn; yuanpei@fzu.edu.cn

How to cite this article: Zhang, B.; Xiao, T.; Hu, C.; Liu, Z.; Chen, P.; Zhao, Z.; Lai, D.; Huang, J.; Zhang, H.; Bao, X.; Yuan, P. Continuous-flow electrooxidation for scalable biomass upgrading over copper-supported CoFe Prussian blue analogues. *Chem. Synth.* **2025**, *5*, 18. https://dx.doi.org/10.20517/cs.2024.37

Received: 21 Mar 2024 **First Decision:** 27 Jun 2024 **Revised:** 14 Jul 2024 **Accepted:** 30 Jul 2024 **Published:** 9 Jan 2025

Academic Editor: Yann Garcia **Copy Editor:** Pei-Yun Wang **Production Editor:** Pei-Yun Wang

Abstract

Electrochemical biomass upgrading is a promising substitute for oxygen evolution reaction (OER) to generate valuable chemicals in conjunction with hydrogen generation. Pursuing highly efficient and durable electrocatalysts for significant concentration levels (≥ 50 mM) of biomass electrooxidation remains an enduring challenge. Herein, we introduce a robust Cu-supported CoFe Prussian blue analogue (CoFe PBA/CF) electrocatalyst, adept at facilitating high-concentration (50 mM) 5-hydroxymethylfurfural (HMF) oxidation into 2,5-furandicarboxylic acid (FDCA), achieving an exceptional HMF conversion (100%) with a notable FDCA yield of 98.4%. The influence of copper substrate and adsorption energy are therefore discussed. Impressively, the CoFe PBA/CF electrode sustains considerable durability in a continuous-flow electrochemical reactor designed for consecutive FDCA production, showcasing FDCA yields of 100/94% at flow rates of 0.4/0.8 mL·min^{-1} over 60 h' uninterrupted electrolysis. This work provides a promising strategy to develop highly efficient and robust electrocatalysts for the consecutive production of high-value products coupled with green H_2 production.

Keywords: 5-hydroxymethylfurfural oxidation, high concentration, structural reconstruction, electrochemical conversion, CoFe Prussian blue analogues

INTRODUCTION

Hydrogen production through electrolytic water splitting is a crucial approach to achieving green and sustainable development[1-4]. However, the sluggish anodic oxygen evolution reaction (OER) kinetics and elevated overpotential pose challenges for water electrolysis, resulting in reduced hydrogen production efficiency and increased energy consumption[5-7]. Considering the significant equilibrium potential [1.23 V *vs.* the reversible hydrogen electrode (RHE)] and elevated overpotential (≥ 190 mV) of OER[8,9], it is necessary to substitute such anodic OER with the electrocatalysis of oxidation reactions that involve small organic molecules, which exhibit more favorable thermodynamics and economic value[10-12]. One such typical reaction is the 5-hydroxymethylfurfural (HMF) electrocatalytic oxidation reaction (HMFOR)[13-15]. The oxidation product (FDCA) serves mainly as a monomer substitute for fossil fuel-derived terephthalic acid in the production of polyethylene terephthalate (PET)[16], and is listed among the top ten most important bio-platform chemicals by the US Department of Energy[17,18].

Recently, transition metal-based electrocatalysts have received considerable attention due to the high conversion, selectivity, and stability in HMFOR[13,15,19-21]. In many studies, small volumes of dilute HMF (≤ 10 mM) are typically utilized in an H-type cell to investigate electrocatalyst characteristics and reaction mechanisms. However, given the fact that high concentration of HMF (≥ 50 mM) is employed in traditional thermochemical oxidation processes[22-24], a HMF solution with elevated concentration is desired to be adopted in the electrocatalytic oxidation process for potential industrial applications. A primary challenge in the electrocatalytic oxidation of high-concentration HMF lies in the fast degradation into humin (by-products) in strong alkali solutions prior to conversion into desired products[25-28]. Therefore, accelerating mass transfer and conversion rates of HMF in the reaction system are crucial to achieving an electrically driven alternative to the traditional thermocatalytic conversion of HMF.

Prussian blue analogue (PBA) derived materials have the advantages of high surface area, uniform porous structure, and structural tunability[29-31]. Studies indicate that PBA materials can be readily reconstituted into ultrathin two-dimensional (2D) hydroxyl oxide nanosheets during electrocatalysis, which is considered as the active phase for HMFOR[32]. Notably, the activity of hydroxyl oxide generated through this approach significantly surpasses that of bulk hydroxyl oxide materials, providing a substantial catalytic advantage[33-35]. Furthermore, recent studies propose that Cu can suppress the deprotonation of OH^* to O^* species and enhance the adsorption and oxidation of aldehyde in HMF, thereby passivating water oxidation activity and enhancing the overall efficiency of HMFOR[36-38]. Therefore, constructing a self-supported PBA catalyst grown on Cu foams is expected to yield elaborately designed catalysts with well-organized structures and highly exposed active sites, which are anticipated to accelerate the HMF adsorption and conversion into desired products[39].

In this study, we developed a self-supported CoFe PBA nanocube propagating on Cu foam (CoFe PBA/CF) via a one-step hydrothermal method for the oxidation of HMF to FDCA under high-concentration conditions (50-100 mM). The integration of Cu substrate not only perpetuates PBA structural regularity and escalates the number of surface-active sites, but also modulates the surface electronic state of Co within the catalyst. This modification augments the adsorption efficiency of HMF on the catalyst surface, thus favoring the electrooxidation process of HMF to FDCA. Moreover, a continuous flow reactor was designed to circumvent the impediments posed by diffusion limitation of high-concentration electrolyte during HMFOR and realize the consecutive production, thus fostering the practical application of the electrocatalytic conversion process from HMF to FDCA.

EXPERIMENTAL

Materials

Cobalt acetate tetrahydrate ($C_4H_6CoO_4·4H_2O$), polyvinylpyrrolidone, and potassium hydroxide (KOH) were purchased from Aladdin Company. Sodium citrate dihydrate ($C_6H_5Na_3O_7·2H_2O$) and potassium ferricyanide ($K_3FeC_6N_6$) were obtained from Macklin Company. Cu foam was purchased from Kunshan Guangjiayuan new material Co., Ltd. Materials 5-hydroxymethyl furfuraldehyde (HMF), 2,5-diformyl furan (DFF), 5-hydroxymethyl-2-furan carboxylic acid (HMFCA), 2,5-furandicarboxylic acid (FDCA) and 5-formyl furan-2-carboxylic acid (FFCA) were obtained from Shanghai Titan Scientific Co., Ltd. Deionized water was used in all experiments, and all the reagents mentioned above were not further treated.

Preparation of CoFe PBA/CF

The synthesis process proceeded as follows: Initially, solution A was prepared by dissolving 0.1 g of cobalt (II) acetate tetrahydrate, 0.14 g of trisodium citrate dihydrate, and 1 g of polyvinylpyrrolidone in 6.5 mL of deionized water. Concurrently, solution B was prepared by dissolving 0.0667 g of potassium hexacyanoferrate (III) in 10 mL of deionized water. Subsequently, solution B was introduced into solution A while subject to magnetic stirring, and the resulting mixture was stirred continuously for 75 s. Following this, the solution obtained, along with a piece of cleaned Cu foam measuring 1 × 2 cm^2, was transferred into a 100 mL Teflon-lined stainless-steel autoclave. The autoclave was sealed and subjected to heating at 100 °C for 16 h. Upon completion of the heating process, the autoclave was allowed to cool to room temperature. The resulting CoFe PBA supported on Cu foam was then washed successively with deionized water and ethanol, and finally dried at 60 °C.

Preparation of CoFe PBA-CF

The remaining solid from the synthesis of CoFe-PBA/CF was collected through centrifugation and subsequently dried under vacuum conditions at 60 °C overnight to obtain CoFe PBA. To prepare the catalyst dispersion, 1.5 mg of the catalysts were combined with 1,000 μL of isopropanol and 20 μL of Nafion solution. This mixture was then subjected to ultrasonication for a duration of 1.5 h. For the fabrication of the working electrode, the as-prepared catalyst dispersion was applied to half of a piece of cleaned Cu foam (1 × 2 cm^2) and left to dry at room temperature to obtain CoFe PBA-CF.

Physical methods

Scanning electron microscopy (SEM) was conducted using a Hitachi S-4800. Transmission electron microscopy (TEM) characterization and elemental mapping measurements were performed on a FEI Tecnai G2 F20. X-ray powder diffraction (XRD) characterization was recorded on a Bruker Corporation D8 ADVANCE with a Cu Kα source (1.54056 Å). X-ray photoelectron spectroscopy (XPS) was conducted using a Thermo Fisher Scientific ESCALAB 25. Fourier transform infrared spectroscopy (FTIR) characterization was recorded on a Thermo Fisher Scientific Nicolet iS50.

In-situ Raman spectroelectrochemical measurement

Raman spectra were obtained utilizing a confocal Raman microscope (Horiba LabRAM HR Evolution) employing a 633 nm excitation wavelength and a 50× objective. Each displayed Raman spectrum was gathered over a 30-second collection period and represents the average of three measurements.

In-situ electrochemical impedance spectroscopy tests

In situ electrochemical impedance spectroscopy (EIS) measurements were carried out in a three-electrode system using the Corrtest electrochemical workstation (CS310X), under the same conditions as OER and HMF oxidation experiments, but without stirring. The frequency range was from 10^4 to 10^{-2} Hz, and the applied potential ranged from 1.2 V to 1.7 V *vs.* RHE with a 0.05 V interval. EIS measurements for OER

were performed in 1 M KOH, while for HMF oxidation, they were conducted in 1 M KOH and 50 mM HMF, respectively.

High-performance liquid chromatography analysis of oxidation products

A 10 μL aliquot was periodically extracted from the electrolyte solution during chronoamperometry at 1.45 V *vs.* RHE and diluted with 990 μL of water. The resulting sample solutions were then analyzed using high-performance liquid chromatography (HPLC, Thermo Fisher Scientific, UltiMate3000) at room temperature to calculate the HMF conversion and yields of oxidation products. The HPLC system was equipped with a 265 nm ultraviolet-visible detector and a 4.6 mm × 250 mm C 18 column. The eluent solvent consisted of a 5 mM ammonium formate aqueous solution and methanol. Separation and quantification were achieved using an isocratic elution of 70% ammonium format and 30% methanol for a 10-minute run time, while the flow rate was set at 0.6 mL·min^{-1}.

The conversion (%) of HMF, the yield (%) of FDCA and Faradaic efficiency (FE) for FDCA production were calculated based on

$$\text{HMF conversion (\%)} = [\frac{m_{con}}{m_{ini}}] \times 100\%$$

$$\text{FDCA yield (\%)} = [\frac{m_{for}}{m_{ini}}] \times 100\%$$

$$\text{FDCA faradaic efficiency (FE) (\%)} = [\frac{(m_{for})\times(n\times F)}{C}] \times 100\%$$

Where m_{con} represents mol of HMF consumed, m_{ini} indicates mol of HMF initial, m_{for} stands for mol of FDCA formed, C points to total charge passed, F denotes Faraday's constant (96,500 C·mol^{-1}), and n is the electron transfer number during the electrooxidation process.

Design of flow reactor

The components of the flow reactor were designed and purchased from Shanghai Chuxi Industrial Co., Ltd. The length, width, height and the wall thickness of the reactor are 4, 4, 4, and 1.5 cm, respectively.

Electrocatalytic experiments

Electrochemical measurements (OER and HMFOR) were conducted using a Corrtest electrochemical workstation (CS310X) potentiostat with a three-electrode configuration in 1 M KOH solution. The Hg/HgO electrode served as the reference electrode. All potentials mentioned in this paper were referenced to the RHE through calibration. The electrochemical experiments (OER and HMFOR) were performed in a 10 mL 1.0 M KOH aqueous solution with and without 50 mM HMF. The cyclic voltammetry (CV) tests are conducted on the CoFe PBA/CF and CoFe PBA-CF catalysts in an alkaline electrolyte to induce their reconstruction. Under alkaline conditions and electric drive etching, the N=C–Fe groups gradually break and leach out. When the CV curves overlap completely (after ~100 cycles), the material reconstruction is complete. Linear sweep voltammetry (LSV) was conducted using the three-electrode configuration at a scan rate of 2 mV·s^{-1}.

For the two-electrode electrolysis in the electrochemical continuous flow reactor, CoFe PBA/CF was used as the anode catalyst, and platinum mesh was used as the cathode catalyst at 1.4 V. The double-layer capacitance (C_{dl}) was determined by analyzing the CV curves obtained in the non-faradaic region at different scan rates.

Density functional theory

All density functional theory (DFT) calculations were conducted by using the Vienna Ab Initio Simulation Package (VASP)[40,41], using the generalized gradient approximation (GGA) of Perdew-Burke-Ernzerhof (PBE) for the exchange-correction functional[42]. The effective U for Co (Ueff = 3.7 eV) was obtained by analyzing the highly localized 3d orbitals of metal ions[43,44]. A cut-off energy of 400 eV was employed. The energy change was < 10^{-5} eV per atom and the iterative process considered was converged when the force on the atom was < 0.03 eV·Å^{-1}. Spin-polarized calculations were incorporated to describe the magnetic properties of Co element.

The CoOOH (001) surface was modeled with p (2 × 2) unit cell and the Brillouin-zone integrations were performed using a (3 × 3 × 1) Monkhorst-Pack mesh during the optimization. The optimized (CoOOH) 4 cluster was placed onto the Cu(111) with p (5 × 5) unit cell of three layers, obtaining the CoOOH/Cu(111) model. The model was simulated using extensive *ab initio* molecular dynamics (AIMD) simulation, and the oscillation amplitude of total energy gets small, indicating that the steady state has been reached and the great stability was confirmed. One OH group was removed to establish surfaces with oxygen vacancy [CoOOH-O_v and CoOOH-O_v/Cu(111)].

The Gibbs free energies (G) at 298.15 K and 1 atm were calculated by:

$$G = H - TS = E_{DFT} + E_{ZPE} + \int_0^{298.15\ K} C_V dT - TS$$

The E_{DFT} and E_{ZPE} represent the total energy obtained from DFT optimization and the zero-point vibrational energy using the harmonic approximation, respectively[45]. C_V, T and S are the heat capacity, kelvin temperature and the entropy, respectively.

RESULTS AND DISCUSSION

Structural and morphological characterizations

The CoFe PBA/CF was synthesized through a hydrothermal synthesis method, exhibiting an evenly distributed and meticulously arrayed continuum of the nanocubes with a diameter of approximately 500 nm [Figure 1A and B]. A high-resolution transmission electron microscope (HRTEM) image reveals these structures uphold a defective cube orientation [Figure 1C] and a lattice spacing of 5.12 Å is observed, which can be attributed to the (200) crystal planes inherently presenting in CoFe PBA (Figure 1C, inset). Energy-dispersive X-ray spectroscopy (EDX) mapping [Figure 1D] illustrates the even distribution of elements on the nanocube, and the inclusion of Cu elements confirms that Cu foam serves not only a supporting role but also facilitates the overall electronic environment of the catalyst. For comparative analysis, powdered CoFe PBA was synthesized using the same method but without growth on Cu foam [Supplementary Figures 1 and 2]. Drip-casting CoFe PBA powder onto the surface of Cu foam (CoFe PBA-CF) resulted in uneven distribution and weak binding between the PBA nanocubes and Cu foam. This comparison suggests that the incorporation of a Cu substrate significantly regularizes the arrangement of PBA nanocubes.

It is well-established that the catalytic efficacy of transition metal derivatives becomes active only after undergoing reconstruction to transform into hydroxides[46,47]. We conducted a detailed comparison of the structural evolution between the CoFe PBA/CF and CoFe PBA-CF electrodes after electric-driven reconstruction in KOH solution [Figure 1E-G, Supplementary Figure 3]. The initially well-aligned PBA nanocubes experienced complete reconstruction, leading to the formation of distinct $Co(OH)_2$ nanosheets. Element mapping [Figure 1H] indicates the presence of Co and Cu elements, while the levels of Fe and N elements significantly decrease in the reconstructed nanosheets. Accompanied by XRD [Figure 1I], FTIR

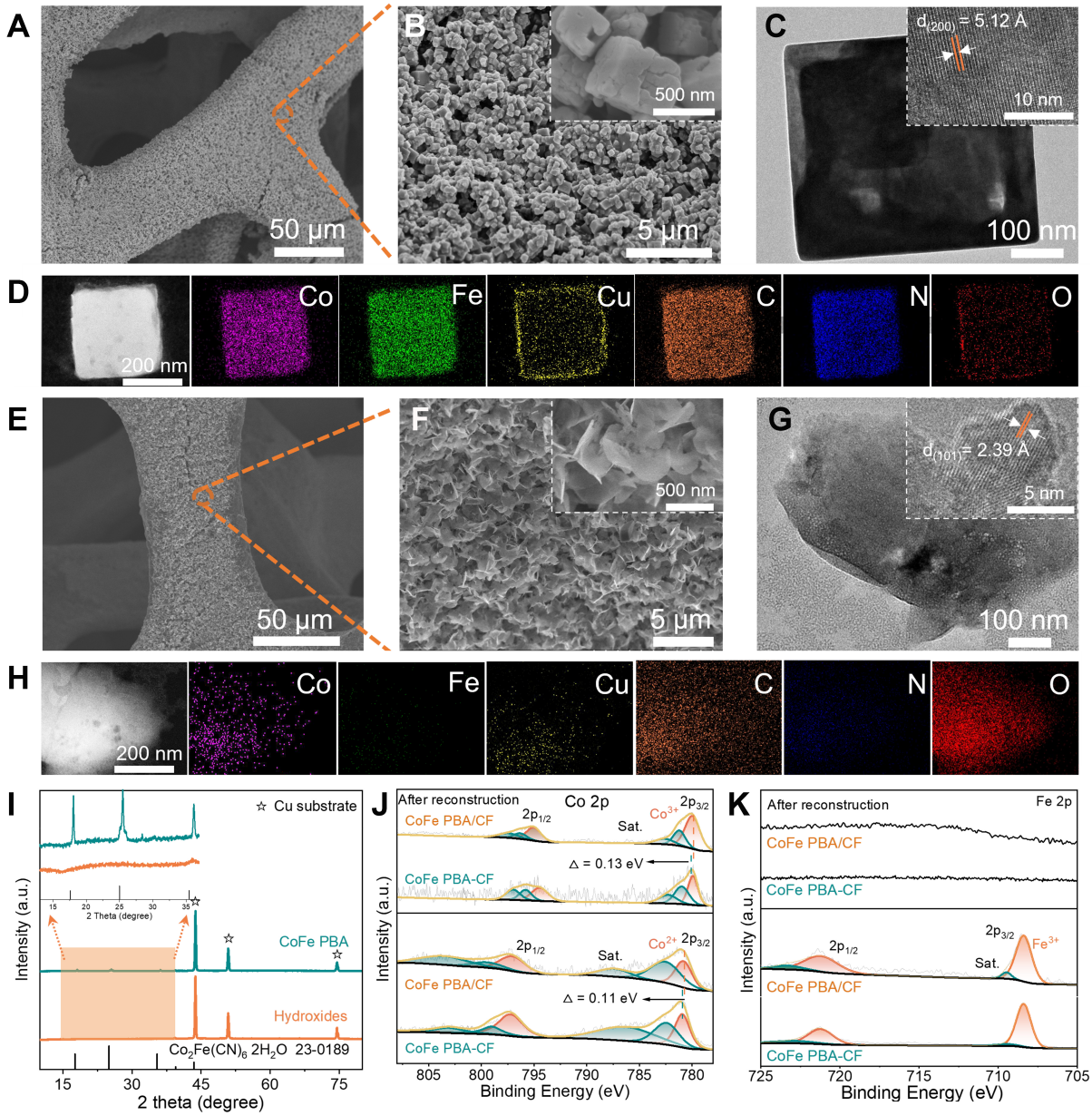

Figure 1. Material characterizations of the CoFe PBA/CF sample. (A and B) SEM, (C) HRTEM images, and (D) EDX mapping; (E and F) SEM, (G) HRTEM images, and (H) EDX mapping after reconstruction in KOH solution; (I) XRD pattern and (J and K) XPS spectra of Co 2p and Fe 2p for CoFe PBA/CF and CoFe PBA-CF samples before and after reconstruction in KOH solution. CoFe PBA/CF: Cu-supported CoFe Prussian blue analogue; SEM: scanning electron microscopy; HRTEM: high-resolution transmission electron microscope; EDX: energy-dispersive X-ray spectroscopy; XRD: X-ray powder diffraction; XPS: X-ray photoelectron spectroscopy.

[Supplementary Figure 4] and inductively coupled plasma (ICP) results [Supplementary Table 1], it can be confirmed that the breakage of Co–N bonds and subsequent dissolution of Fe species occur during the reconstruction of PBA to amorphous hydroxides. Surface electronic states were further characterized by XPS. The peaks for Co $2p_{3/2}$ and $2p_{1/2}$ were observed at around 780.8 and 797.4 eV [Figure 1J], while Fe $2p_{1/2}$ and $2p_{3/2}$ were located at 721.4 and 708.4 eV, respectively [Figure 1K]. Specifically, the Co $2p_{2/3}$ spectrum could be decomposed and assigned to Co–N (780.8 eV) and Co–O (783.0 eV) species[48,49]. Compared to CoFe PBA-CF, CoFe PBA/CF exhibited a negative shift of 0.11 eV, indicating the electron-rich properties of

Cu-induced surface Co species, which persisted even after reconstruction. However, no Fe species was detected [Supplementary Figure 5], suggesting the dissolution of Fe atoms during reconstruction of PBA, consistent with the EDX [Supplementary Figure 6] and ICP results. Therefore, we infer that the active species for HMF oxidation mainly originates from the Co-based hydroxides during the electrocatalytic reaction.

HMFOR performance of the surface reconstructed CoFe PBA/CF electrode

An H-type electrochemical cell, utilizing 1.0 M KOH as the cathodic electrolyte and a solution containing 50 mM HMF in 1.0 M KOH as the anodic electrolyte, was employed to assess the electrochemical HMFOR performance of CoFe PBA/CF and CoFe PBA-CF [Supplementary Figure 7]. LSV curves were measured at a scan rate of 2 $mV \cdot s^{-1}$ to compare the competing reactions between OER and HMFOR [Figure 2A, Supplementary Figure 8]. The self-supported CoFe PBA/CF electrode exhibited the lowest potential of 1.20/1.38 V *vs.* RHE at 10/100 $mA \cdot cm^{-2}$ for HMF oxidation (50 mM in 1 M KOH) compared to the CoFe PBA-CF electrode (1.30/1.53 V *vs.* RHE) and the condition without HMF (1.45/1.60 V *vs.* RHE). To further elucidate the interfacial electrochemical behavior during the catalytic process, *in situ* EIS was conducted, and the corresponding Bode phase plots are presented in Figure 2B and C. The low-frequency region (10^{-2} to 10^{1} Hz) is related to the nonhomogeneous charge distribution, specifically the appearance of oxidation species at the electrode interface[50,51]. A peak is found in the low-frequency region at 1.45 V either with or without HMF, indicating OER occurs at the electrode surface. The introduction of HMF results in an additional peak at 1.25 V, indicating HMF oxidation occurs at this voltage level. Combined LSV and EIS analyses confirm that the suitable electrocatalytic HMFOR range is 1.20 to 1.45 V, during which the occurrence of OER side reactions is avoided.

Moreover, the CoFe PBA/CF electrode also delivered a considerably smaller Tafel slope at 116.54 $mV \cdot dec^{-1}$ compared to CoFe PBA-CF at 167.46 $mV \cdot dec^{-1}$, suggesting that the intrinsic HMFOR reaction kinetics could be enhanced via the chemical interaction between the PBA nanocubes and the Cu foam substrate [Figure 2D]. The reaction rates of HMF with various concentrations were further evaluated to ascertain the intrinsic activity of CoFe PBA towards HMFOR [Figure 2E, Supplementary Figure 9]. For CoFe PBA/CF, a steady conversion rate of 3.8 $mM \cdot min^{-1}$ was achieved when the HMF concentration was approximately 70 mM, whereas CoFe PBA-CF could only reach a rate of 1.22 $mM \cdot min^{-1}$. Further investigation involved recording CV within the non-faradaic potential range of 1.0 to 1.1 V [Supplementary Figure 10] to calculate the C_{dl}. The DLC for CoFe PBA/CF was significantly higher, at 376.18 $mF \cdot cm^{-2}$, which is 3.58 times that of CoFe PBA-CF (105.01 $mF \cdot cm^{-2}$), implies that the quantity of active sites in the self-supported CoFe PBA/CF considerably outnumbers those in CoFe PBA-CF. Based on these results, we can confirm that the well-aligned self-supported structure not only provides an increased number of reaction sites for HMF conversion but also enhances the intrinsic electrocatalytic activity through the concurrent introduction of a Cu substrate.

HPLC was utilized to analyze and quantify the oxidation products following HMFOR. At the potential of 1.45 V, HMF underwent rapid conversion to FDCA, ultimately attaining 100% HMF conversion with a yield of 98.4% and 98% FE towards FDCA production [Figure 2F]. By contrast, the powder CoFe PBA-CF can only achieve an 85.7% conversion, 69% selectivity, and 84% FE. The durability of CoFe PBA/CF was further clarified by conducting cycling experiments [Figure 2G, Supplementary Figure 11]. Impressively, even after 20 cycles, HMF conversion remained stable at 100%, and FDCA productivity sustained at approximately 90%. This stability suggests that CoFe PBA/CF demonstrates high activity, excellent FDCA selectivity, and remarkable catalytic recyclability owing to its regular structure and complete exposure of active sites, even in a strong alkali environment. Additionally, we monitored the hydrogen evolution during the HMFOR process [Supplementary Video 1], observing a significant hydrogen generation. The calculated hydrogen

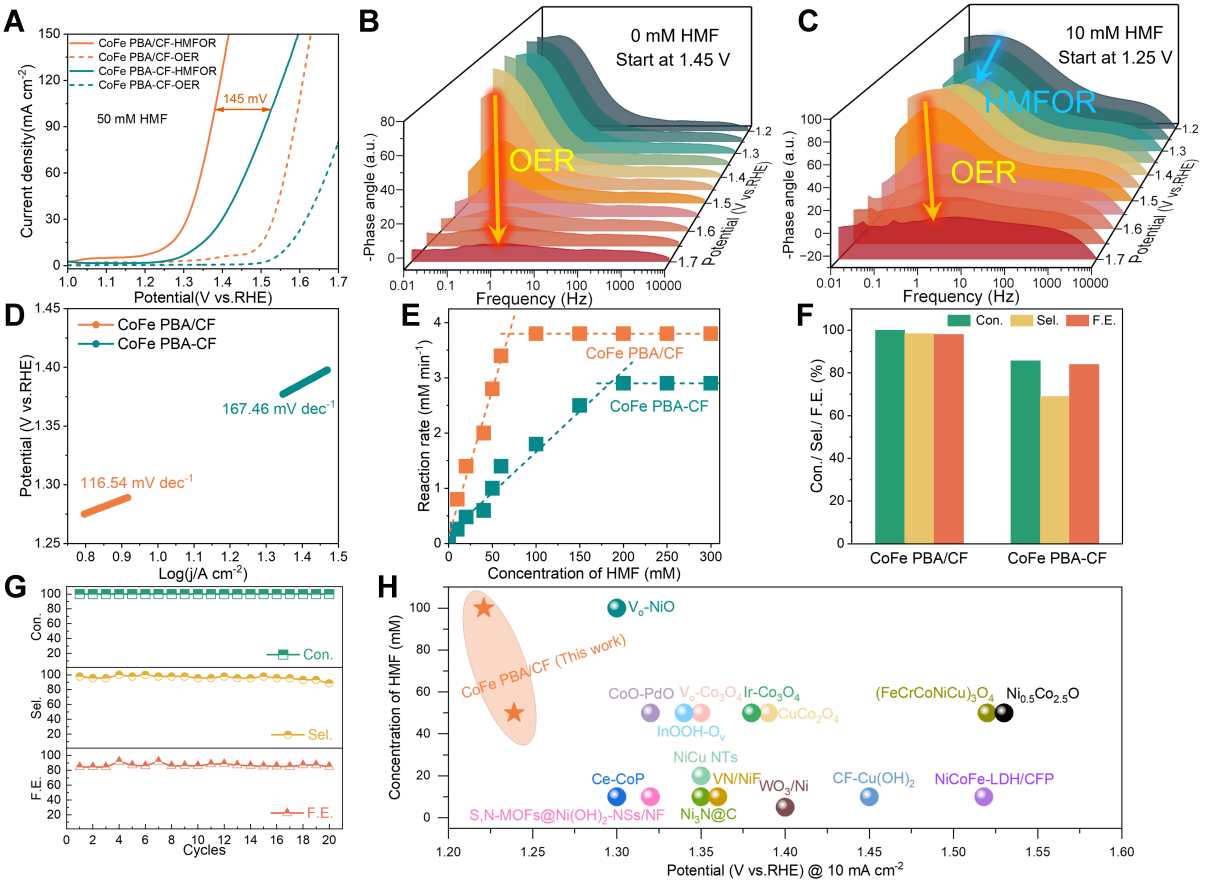

Figure 2. (A) LSV curves of CoFe PBA/CF and CoFe PBA-CF samples in 1M KOH with 50 mM HMF and without HMF; (B and C) Bode phase plots of CoFe PBA/CF sample; (D) Tafel plots of CoFe PBA/CF and CoFe PBA-CF electrodes; (E) HMF reaction rate of CoFe PBA/CF and CoFe PBA-CF electrodes with varying HMF concentrations; (F) Comparison of HMF conversion, FDCA yield, and FE between CoFe PBA/CF and CoFe PBA-CF; (G) Durability test for CoFe PBA/CF sample; (H) Comparison of overpotential for CoFe PBA/CF with other reported catalysts. LSV: Linear sweep voltammetry; CoFe PBA/CF: Cu-supported CoFe Prussian blue analogue; HMF: 5-hydroxymethylfurfural; FDCA: 2,5-furandicarboxylic acid; FE: Faradaic efficiency.

generation rate is approximately 1.1 mL·min^{-1}, with the transferred charge quantity closely matching the detected anode values. Notably, the superior electrocatalytic activity observed for CoFe PBA/CF surpasses those previously reported transition oxides derivate catalysts for HMFOR to FDCA in the last three years [Supplementary Table 2, Figure 2H].

The reaction mechanism and DFT calculations

Two possible reaction pathways for HMF oxidation are illustrated in Figure 3A, including the initial alcohol hydroxyl oxidation to DFF and the aldehyde oxidation to HMFCA, respectively[52,53]. As the reaction proceeded, the content of HMF diminished gradually, while the content of intermediates, namely HMFCA and FFCA, increased at initial stage and declined towards the end of the reaction [Figure 3B, Supplementary Figure 12]. This outcome suggests that the reaction follows an HMF-HMFCA-FFCA-FDCA pathway with the CoFe PBA/CF catalyst. In addition, we conducted a quantitative analysis of the oxidative products. Chronoamperometric electrolysis was performed at a constant voltage of 1.45 V to input a theoretical charge of 289.5 C with an HMF concentration of 50 mM [Figure 3C]. It is observed that the content of HMF considerably drops during the initial 100 C, accompanied by the formation of HMFCA and FDCA. Notably, the intermediate FFCA maintained a very low presence throughout the reaction, hinting that the transition

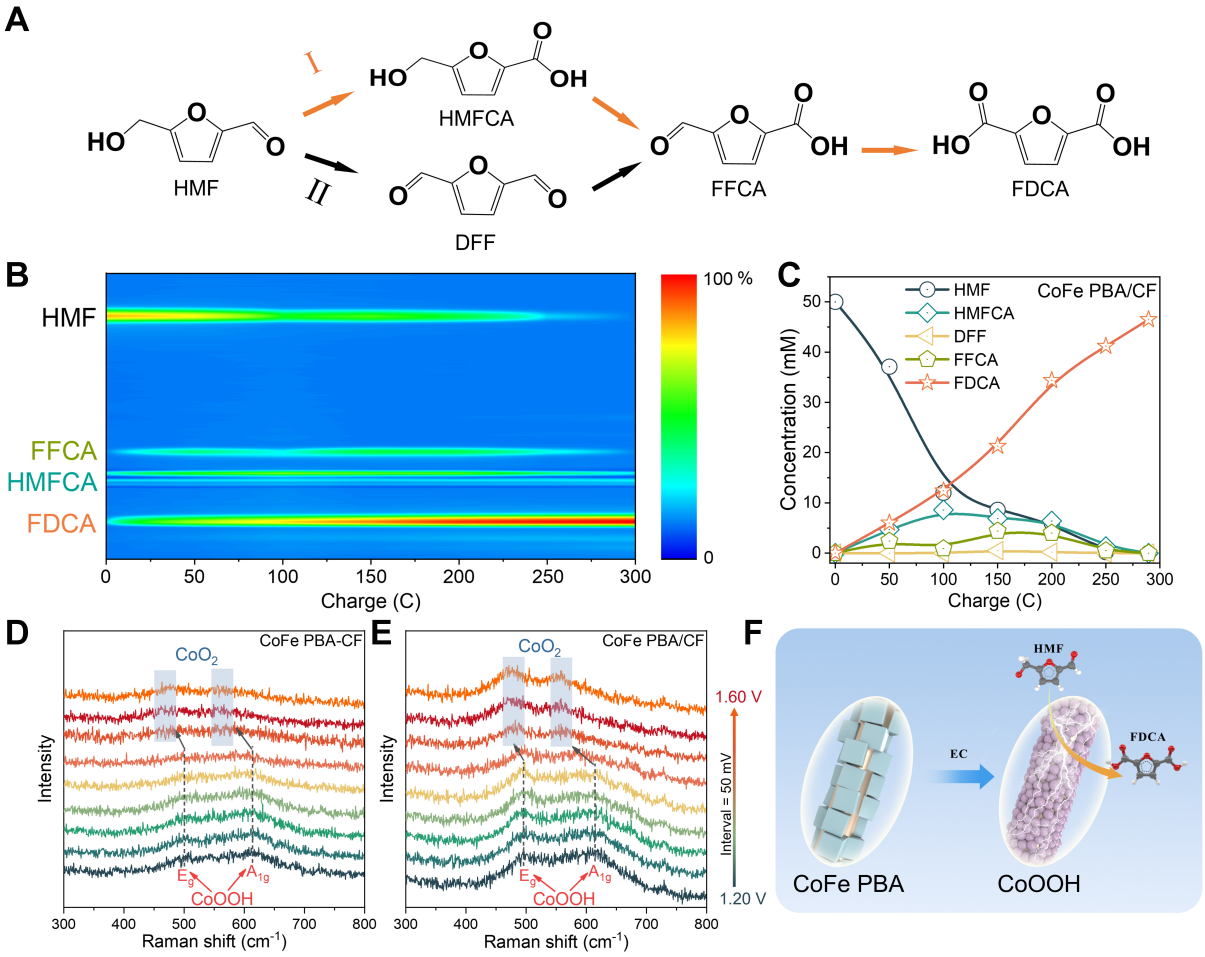

Figure 3. (A) Two possible reaction pathways for HMF electrooxidation; (B and C) Concentration changes of the reactant and products during HMFOR at 1.45 V; (D and E) *In situ* Raman spectra of HMFOR process on CoFe PBA-CF and CoFe PBA/CF sample; (F) Illustration of transformation of electrocatalyst and the electrooxidation of HMF on reactive sites. HMF: 5-hydroxymethylfurfural; HMFOR: 5-hydroxymethylfurfural electrocatalytic oxidation reaction; CoFe PBA/CF: Cu-supported CoFe Prussian blue analogue.

from HMFCA to FDCA occurred rapidly.

In-situ electrochemical Raman spectroscopy was used to identify the active phase of catalysts during the HMFOR[32,54]. The experiments involved a preliminary 10-minute electrolysis before measuring Raman spectra to ensure the conditions as close as possible to the true reaction environment. Two broad spectral features at 497 and 609 cm^{-1} were detected on both CoFe PBA-CF and CoFe PBA/CF samples, which can be attributed to the E_g and A_{1g} vibration modes of Co^{3+}–O bonds, respectively [Figure 3D and E]. The higher relative intensity observed on the CoFe PBA/CF electrode indicates that CoFe PBA *in-situ* grown on the Cu substrate tends to reconstruct more thoroughly, forming abundant active sites when driven by the potential in alkaline conditions. It is noticed that the peaks remained unchanged until the potential reached 1.45 V, suggesting that the active phase for HMFOR exclusively involves CoOOH when the current density reaches 100 $mA·cm^{-2}$ (1.380 V). Moreover, these peaks gradually red-shifted to 474 and 558 cm^{-1} when the potential reached 1.50 V and weakened further upon incrementing potential. This red shift can be assigned to the Co–O bands of CoO_2 species, pointing to structural instability under such intensified potential conditions[55,56]. Based on these findings, we infer the excellent performance of CoFe PBA/CF electrodes can

be attributed to the following fact: the overoxidation of the catalyst to form CoO_2 species that may lead to structural degradation is avoided under the selected potential (1.45 V); instead, the catalyst is activated to form CoOOH exactly, which serves as the oxidant to drives the rapid conversion of HMF into FDCA [Figure 3F].

DFT simulations were conducted to deepen our understanding of the promotion effect of the Cu substrate on HMFOR. Observations revealed a lower Bader charge for the Co site on CoOOH/Cu(111) (+0.670 |e|) compared to that on the CoOOH surface (+1.178 |e|), implying electron transfer from the Cu substrate to the Co sites [Figure 4A and B]. Simultaneously, the region around the Co^{x+} site of CoOOH/Cu(111) exhibited the most positive electrostatic potential value, making it easier for reactants to adsorb. Thus, we calculated the adsorption energies of HMF at different Co^{x+} sites. Considering that the oxygen atoms of formyl (-CHO) in HMF act as electron acceptors, they show a preference for adsorption on electron-rich Co sites from the CoOOH/Cu(111) surface. Notably, the adsorption energy of HMF on CoOOH/Cu(111) is -1.00 eV, significantly greater than that on the CoOOH (-0.52 eV) surface [Supplementary Figures 13-15]. This observation suggests that the introduction of Cu substrate facilitates the absorption of HMF molecules.

We further conducted studies on Gibbs free energy evolutions for HMFOR to FDCA conversion both on CoOOH and CoOOH/Cu(111) surfaces [Figure 4C] to elucidate the differences in electrocatalytic performance for HMF oxidation. The results demonstrate that the ΔG values for the HMFOR elementary processes on both CoOOH and CoOOH/Cu(111) are thermodynamically favorable. The larger free energy gap observed in the step from HMFCA to FFCA on CoOOH/Cu(111) (-0.90 eV), compared to that for HMF to HMFCA on CoOOH (-0.25 eV), suggests that the active site exhibits reduced charge transfer, catalyzes the dehydrogenation step of HMF and thereby modifies the reaction kinetics. Therefore, CoOOH/Cu(111), with its large Gibbs free energy gap for the potential path and adsorption energy of HMF, is more favorable for the conversion of HMF compared to CoOOH. Based on the theoretical results, we can infer that the electronic redistribution between Co and Cu facilitates the catalytic progress for HMFOR, which is consistent with the experimental observations.

Continuous flow electrooxidation of HMF to FDCA

Considering the industrial applications, the production of FDCA should ideally operate continuously within a practical reactor[19,21,57,58]. Importantly, improving the mass transfer of the electrolyte is critical to the electrochemical reaction, particularly when the reactant concentration is high (≥ 50 mM). In a traditional H-type cell, the reactant species on the active sites are not easy to refresh timely for fast conversion and the reaction of different benches of feedstock is intermittent, thus significantly reducing the production efficiency. To achieve consecutive and efficient production of FDCA from concentrated HMF solution, we have developed a continuous-flow electrochemical reactor (CFER) [Figure 5A]. The KOH and HMF solutions are independently delivered and subsequently mixed in a tee valve before being pumped into the CFER. This setup enables the rapid conversion of the reactive substrate into the targeted product within the CFER, effectively preventing the degradation of HMF in the KOH solution. Notably, both the conversion and selectivity of HMF to FDCA remained remarkably high at close to 100% at the flow rate of 0.4 $mL \cdot min^{-1}$ [Figure 5B]. The procedure entailing the continuous oxidation of high-concentration HMF to FDCA via the CFER was documented through videography [Supplementary Video 2]. Observations from the video, in conjunction with Supplementary Figure 16, divulge that the yellow-hued HMF solution amalgamates with KOH in the tee valve and subsequently engenders a colorless FDCA solution in CFER.

Furthermore, an escalated flow rate (0.8 $mL \cdot min^{-1}$) delivered continued HMF conversions of approximately 99%, while the selectivity for FDCA remained stable at around 94%. Such superior performance infers that

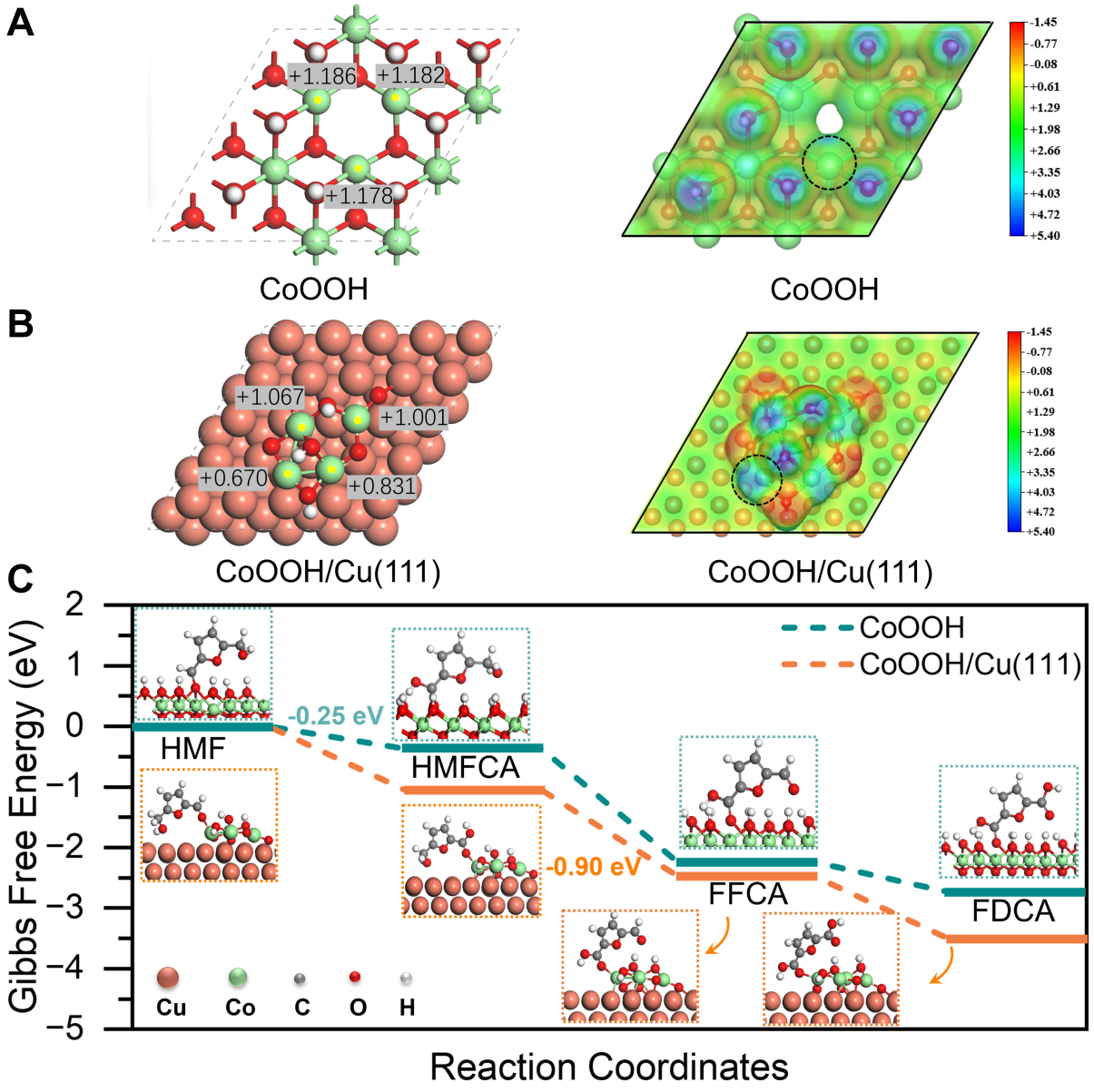

Figure 4. (A and B) Top-view diagrams of constructed models for CoOOH, CoOOH/Cu(111), including the corresponding Bader charge transfer (|e|) and electrostatic potentials with an isosurface value of 0.003 e/Bohr^3; (C) Free energy diagram for HMFOR on both CoOOH and CoOOH/Cu(111), illustrating the adsorption configurations of intermediates. HMFOR: 5-hydroxymethylfurfural electrocatalytic oxidation reaction.

the CoFe PBA/CF catalyst is capable of swiftly converting HMF, thereby demonstrating its capacity to effectively handle high concentrations of HMF during the reaction process. We also assessed the durability of the CoFe PBA/CF electrodes [Figure 5C, Supplementary Figure 17]. Even after enduring over 60 h of continuous electrolysis within the CFER, these electrodes still maintained impressive HMF conversion rates (close to 100%) and FDCA selectivity (97%), signifying the durability and promising productivity potential. Moreover, we monitored structural transformations of the PBA over various time periods during the HMFOR reaction to explore the correlation between its elevated stability and structural changes (Figure 5C, inset, Supplementary Figures 18 and 19). CoFe PBA/CF was transformed into $Co(OH)_2$ nanosheets and demonstrated prolonged structural stability during HMFOR. Accordingly, these results suggest the

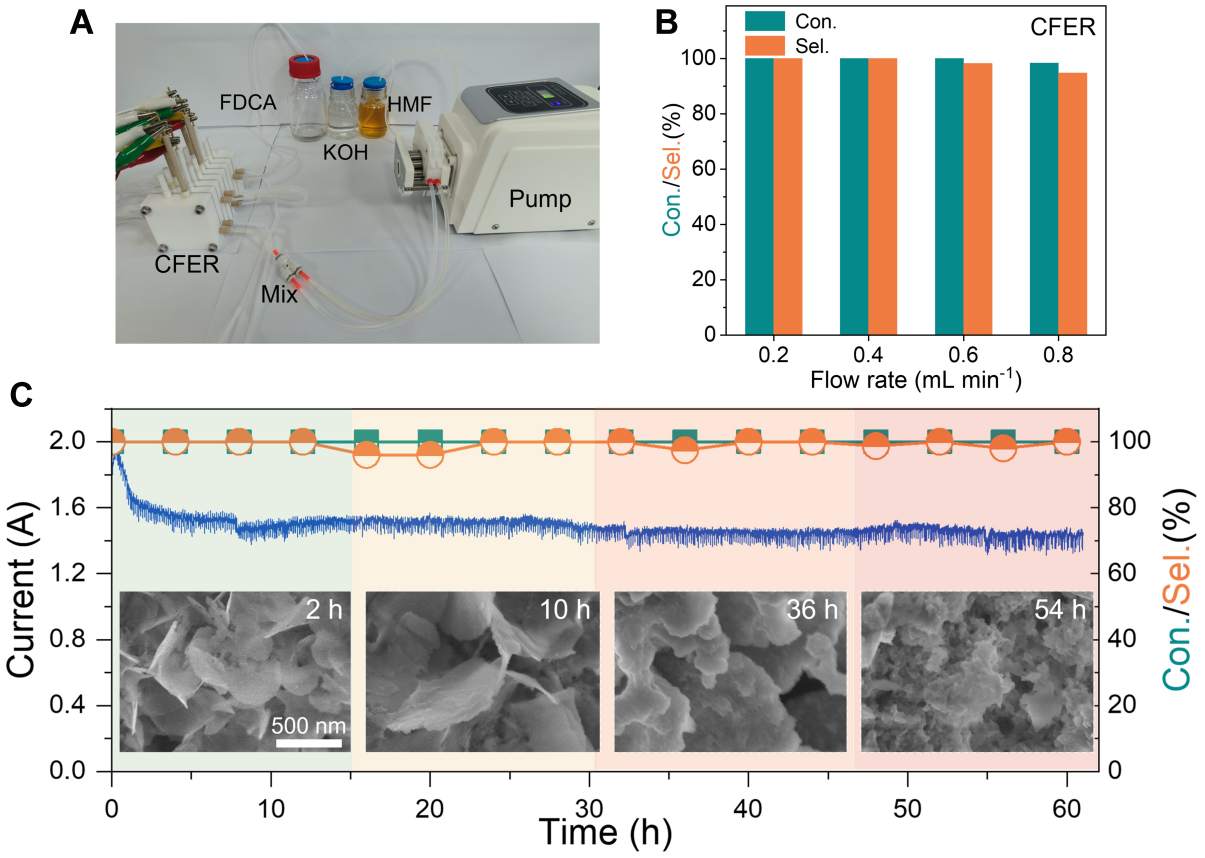

Figure 5. (A) Photographic image of the CFER for HMFOR; (B) HMF conversion and FDCA selectivity at various flow rates; (C) Durability test of CoFe-PBA/CF in the CFER at the potential of 1.4 V with 50 mM HMF in 1 M KOH solution as the electrolyte. CFER: Continuous-flow electrochemical reactor; HMFOR: 5-hydroxymethylfurfural electrocatalytic oxidation reaction; HMF: 5-hydroxymethylfurfural; FDCA: 2,5-furandicarboxylic acid; CoFe PBA/CF: Cu-supported CoFe Prussian blue analogue.

immense potential of our CoFe PBA/CF electrodes and the engineered CFER for facilitating the continuous, large-scale production of FDCA under industrial conditions.

CONCLUSIONS

In summary, a robust self-supported CoFe PBA/CF electrocatalyst has been constructed via a hydrothermal process. The self-supported CoFe PBA/CF demonstrates superb HMFOR electrocatalytic performance, achieving a remarkable 98.4% yield of FDCA and a 98% FE when subjected to high-concentration HMF solutions (≥ 50 mM), representing a significant enhancement compared to current low-dose HMF conversion processes. DFT theoretical calculations and series characterizations show that the introduction of Cu substrate not only improves PBA structural regularity and the number of surface-active sites, but also regulates the surface electronic state of Co in the catalyst, thereby facilitating the adsorption and conversion of HMF. Impressively, a continuous flow electrochemical reactor is designed to accelerate the diffusion, thereby enabling operation at high reaction rates. This design achieves a yield of FDCA close to 97% during the continuous 60-hour reaction. Our contribution paves the way for biomass upgrading to produce value-added products by constructing high-performance self-supported electrodes and coupling them with a continuous flow reactor.

DECLARATIONS

Authors' contributions

Designed, prepared and revised the manuscript: Zhang B, Hu C, Zhang H, Yuan P

Discussion and preparation of the manuscript: Zhang B, Xiao T, Hu C, Liu Z, Chen P, Zhao Z, Lai D, Huang J, Zhang H, Bao X, Yuan P

Availability of data and materials

Not applicable.

Financial support and sponsorship

This work is supported by the National Key R&D Project (2022YFB4004100), National Natural Science Foundation of China, Pilot Group Program of the Research Fund for International Senior Scientists (22250710676), National Natural Science Foundation of China (22078064, 22304028), and Natural Science Foundation of Fujian Province (2021J02009).

Conflicts of interest

All authors declared that there are no conflicts of interest.

Ethical approval and consent to participate

Not applicable.

Consent for publication

Not applicable.

REFERENCES

1. Gao, G.; Zhu, G.; Chen, X.; Sun, Z.; Cabot, A. Optimizing Pt-based alloy electrocatalysts for improved hydrogen evolution performance in alkaline electrolytes: a comprehensive review. *ACS. Nano.* **2023**, *17*, 20804-24. DOI PubMed
2. Wang, J.; Yue, X.; Yang, Y.; et al. Earth-abundant transition-metal-based bifunctional catalysts for overall electrochemical water splitting: a review. *J. Alloys. Compd.* **2020**, *819*, 153346. DOI
3. Yang, Q.; Liu, H.; Yuan, P.; et al. Single carbon vacancy traps atomic platinum for hydrogen evolution catalysis. *J. Am. Chem. Soc.* **2022**, *144*, 2171-8. DOI PubMed
4. Liu, W.; Niu, X.; Tang, J.; et al. Energy-efficient anodic reactions for sustainable hydrogen production via water electrolysis. *Chem. Synth.* **2023**, *3*, 44. DOI
5. Zhuang, L.; Jia, Y.; Liu, H.; et al. Sulfur-modified oxygen vacancies in iron-cobalt oxide nanosheets: enabling extremely high activity of the oxygen evolution reaction to achieve the industrial water splitting benchmark. *Angew. Chem. Int. Ed. Engl.* **2020**, *59*, 14664-70. DOI PubMed
6. Wang, B.; Chen, X.; He, Y.; et al. Fe_2O_3/P-doped $CoMoO_4$ electrocatalyst delivers efficient overall water splitting in alkaline media. *Appl. Catal. B. Environ.* **2024**, *346*, 123741. DOI
7. Wang, C.; Jiang, X.; Wang, Y.; Tang, Y.; Zhou, J.; Fu, G. Recent advances in nonmetallic modulation of palladium-based electrocatalysts. *Chem. Synth.* **2023**, *3*, 8. DOI
8. Zhang, J.; Zhang, Q.; Feng, X. Support and interface effects in water-splitting electrocatalysts. *Adv. Mater.* **2019**, *31*, e1808167. DOI PubMed
9. Walter, M. G.; Warren, E. L.; McKone, J. R.; et al. Solar water splitting cells. *Chem. Rev.* **2010**, *110*, 6446-73. DOI PubMed
10. Urbańczyk, E.; Maciej, A.; Stolarczyk, A.; Basiaga, M.; Simka, W. The electrocatalytic oxidation of urea on nickel-graphene and nickel-graphene oxide composite electrodes. *Electrochim. Acta.* **2019**, *305*, 256-63. DOI
11. Hu, S.; Wang, B.; Ma, Y.; Li, M.; Zhang, L.; Huang, Z. Ultrathin bismuth tungstate nanosheets as an effective photo-assisted support for electrocatalytic methanol oxidation. *J. Colloid. Interface. Sci.* **2019**, *552*, 179-85. DOI PubMed
12. Barwe, S.; Weidner, J.; Cychy, S.; et al. Electrocatalytic oxidation of 5-(hydroxymethyl)furfural using high-surface-area nickel boride. *Angew. Chem. Int. Ed. Engl.* **2018**, *57*, 11460-4. DOI PubMed
13. Zhang, N.; Zou, Y.; Tao, L.; et al. Electrochemical oxidation of 5-hydroxymethylfurfural on nickel nitride/carbon nanosheets: reaction

pathway determined by in situ sum frequency generation vibrational spectroscopy. *Angew. Chem. Int. Ed. Engl.* **2019**, *58*, 15895-903. DOI PubMed

14. Xu, H.; Xin, G.; Hu, W.; et al. Single-atoms Ru/NiFe layered double hydroxide electrocatalyst: efficient for oxidation of selective oxidation of 5-hydroxymethylfurfural and oxygen evolution reaction. *Appl. Catal. B. Environ.* **2023**, *339*, 123157. DOI
15. Luo, R.; Li, Y.; Xing, L.; et al. A dynamic $Ni(OH)_2$-NiOOH/NiFeP heterojunction enabling high-performance E-upgrading of hydroxymethylfurfural. *Appl. Catal. B. Environ.* **2022**, *311*, 121357. DOI
16. Zhang, B.; Fu, H.; Mu, T. Hierarchical NiS_x/Ni_2P nanotube arrays with abundant interfaces for efficient electrocatalytic oxidation of 5-hydroxymethylfurfural. *Green. Chem.* **2022**, *24*, 877-84. DOI
17. Bozell, J. J.; Petersen, G. R. Technology development for the production of biobased products from biorefinery carbohydrates - the US Department of Energy's "Top 10" revisited. *Green. Chem.* **2010**, *12*, 539-54. DOI
18. Werpy, T.; Petersen, G.; Aden, A.; et al. Top value added chemicals from biomass. Volume 1: results of screening for potential candidates from sugars and synthesis gas. 2004. Available from: https://www.rivertop.com/files/bioenergy/pdfs/35523.pdf. [Last accessed on 29 Aug 2024]
19. Wang, H.; Zhou, Y.; Tao, S. CoP-CoOOH heterojunction with modulating interfacial electronic structure: a robust biomass-upgrading electrocatalyst. *Appl. Catal. B. Environ.* **2022**, *315*, 121588. DOI
20. Zhou, P.; Lv, X.; Tao, S.; et al. Heterogeneous-interface-enhanced adsorption of organic and hydroxyl for biomass electrooxidation. *Adv. Mater.* **2022**, *34*, e2204089. DOI PubMed
21. Wang, H.; Zhang, J.; Tao, S. Nickel oxide nanoparticles with oxygen vacancies for boosting biomass-upgrading. *Chem. Eng. J.* **2022**, *444*, 136693. DOI
22. Nie, J.; Liu, H. Efficient aerobic oxidation of 5-hydroxymethylfurfural to 2,5-diformylfuran on manganese oxide catalysts. *J. Catal.* **2014**, *316*, 57-66. DOI
23. Nie, J.; Xie, J.; Liu, H. Activated carbon-supported ruthenium as an efficient catalyst for selective aerobic oxidation of 5-hydroxymethylfurfural to 2,5-diformylfuran. *Chinese. J. Catal.* **2013**, *34*, 871-5. DOI
24. Wei, Y.; Zhang, Y.; Chen, Y.; et al. Crystal faces-tailored oxygen vacancy in Au/CeO_2 catalysts for efficient oxidation of HMF to FDCA. *ChemSusChem* **2022**, *15*, e202101983. DOI PubMed
25. Vuyyuru, K. R.; Strasser, P. Oxidation of biomass derived 5-hydroxymethylfurfural using heterogeneous and electrochemical catalysis. *Catal. Today.* **2012**, *195*, 144-54. DOI
26. Nam, D.; Taitt, B. J.; Choi, K. Copper-based catalytic anodes to produce 2,5-furandicarboxylic acid, a biomass-derived alternative to terephthalic acid. *ACS. Catal.* **2018**, *8*, 1197-206. DOI
27. Patil, S. K. R.; Lund, C. R. F. Formation and growth of humins via aldol addition and condensation during acid-catalyzed conversion of 5-hydroxymethylfurfural. *Energy. Fuels.* **2011**, *25*, 4745-55. DOI
28. van, Z. I.; Wang, Y.; Rasrendra, C. B.; et al. Formation, molecular structure, and morphology of humins in biomass conversion: influence of feedstock and processing conditions. *ChemSusChem* **2013**, *6*, 1745-58. DOI PubMed
29. Duan, J.; Chen, S.; Zhao, C. Ultrathin metal-organic framework array for efficient electrocatalytic water splitting. *Nat. Commun.* **2017**, *8*, 15341. DOI PubMed PMC
30. Indra, A.; Paik, U.; Song, T. Boosting electrochemical water oxidation with metal hydroxide carbonate templated prussian blue analogues. *Angew. Chem. Int. Ed. Engl.* **2018**, *57*, 1241-5. DOI PubMed
31. Zhou, J.; Wang, Y.; Su, X.; et al. Electrochemically accessing ultrathin Co (oxy)-hydroxide nanosheets and *operando* identifying their active phase for the oxygen evolution reaction. *Energy. Environ. Sci.* **2019**, *12*, 739-46. DOI
32. Zhou, B.; Li, Y.; Zou, Y.; et al. Platinum modulates redox properties and 5-hydroxymethylfurfural adsorption kinetics of $Ni(OH)_2$ for biomass upgrading. *Angew. Chem. Int. Ed. Engl.* **2021**, *60*, 22908-14. DOI PubMed
33. Zhuang, L.; Ge, L.; Yang, Y.; et al. Ultrathin iron-cobalt oxide nanosheets with abundant oxygen vacancies for the oxygen evolution reaction. *Adv. Mater.* **2017**, *29*, 1606793. DOI PubMed
34. Song, F.; Hu, X. Exfoliation of layered double hydroxides for enhanced oxygen evolution catalysis. *Nat. Commun.* **2014**, *5*, 4477. DOI PubMed
35. Das, T. K.; Jesionek, M.; Çelik, Y.; Poater, A. Catalytic polymer nanocomposites for environmental remediation of wastewater. *Sci. Total. Environ.* **2023**, *901*, 165772. DOI PubMed
36. Chen, D.; Ding, Y.; Cao, X.; et al. Highly efficient biomass upgrading by a Ni-Cu electrocatalyst featuring passivation of water oxidation activity. *Angew. Chem. Int. Ed. Engl.* **2023**, *62*, e202309478. DOI PubMed
37. Pang, X.; Bai, H.; Zhao, H.; Fan, W.; Shi, W. Efficient electrocatalytic oxidation of 5-hydroxymethylfurfural coupled with 4-nitrophenol hydrogenation in a water system. *ACS. Catal.* **2022**, *12*, 1545-57. DOI
38. Woo, J.; Moon, B. C.; Lee, U.; et al. Collaborative electrochemical oxidation of the alcohol and aldehyde groups of 5-hydroxymethylfurfural by NiOOH and $Cu(OH)_2$ for superior 2,5-furandicarboxylic acid production. *ACS. Catal.* **2022**, *12*, 4078-91. DOI
39. Zhao, G.; Hai, G.; Zhou, P.; et al. Electrochemical oxidation of 5-hydroxymethylfurfural on CeO_2-modified Co_3O_4 with regulated intermediate adsorption and promoted charge transfer. *Adv. Funct. Mater.* **2023**, *33*, 2213170. DOI
40. Kresse, G.; Furthmüller, J. Efficient iterative schemes for ab initio total-energy calculations using a plane-wave basis set. *Phys. Rev. B. Condens. Matter.* **1996**, *54*, 11169-86. DOI PubMed
41. Kresse, G.; Hafner, J. Ab initio molecular-dynamics simulation of the liquid-metal-amorphous-semiconductor transition in germanium.

Phys. Rev. B. Condens. Matter. **1994**, *49*, 14251-69. DOI PubMed

42. Perdew, J. P.; Burke, K.; Ernzerhof, M. Generalized gradient approximation made simple [Phys. Rev. Lett. 77, 3865 (1996)]. *Phys. Rev. Lett.* **1997**, *78*, 1396. DOI
43. Liechtenstein, A. I.; Anisimov, V. I. V. I.; Zaanen, J. Density-functional theory and strong interactions: orbital ordering in Mott-Hubbard insulators. *Phys. Rev. B. Condens. Matter.* **1995**, *52*, R5467-70. DOI PubMed
44. Jamal, M.; Shahriyar, N. S.; Sharif, A. Effects of transition metal (Fe, Co & Ni) doping on structural, electronic and optical properties of CuO: DFT + U study. *Chem. Phys.* **2021**, *545*, 111160. DOI
45. Heinz, U.; Song, H.; Chaudhuri, A. K. Dissipative hydrodynamics for viscous relativistic fluids. *Phys. Rev. C.* **2006**, *73*, 034904. DOI
46. Wang, H.; Niu, C.; Liu, W.; Tao, S. d-Electron tuned CoMoP for enhance 5-hydroxymethylfurfural oxidation and HER. *Appl. Catal. B. Environ.* **2024**, *340*, 123249. DOI
47. Wu, T.; Xu, Z.; Wang, X.; et al. Surface-confined self-reconstruction to sulfate-terminated ultrathin layers on $NiMo_3S_4$ toward biomass molecule electro-oxidation. *Appl. Catal. B. Environ.* **2023**, *323*, 122126. DOI
48. Cai, X.; Peng, F.; Luo, X.; et al. Understanding the evolution of cobalt-based metal-organic frameworks in electrocatalysis for the oxygen evolution reaction. *ChemSusChem* **2021**, *14*, 3163-73. DOI PubMed
49. Hu, L.; Hu, Y.; Liu, R.; Mao, Y.; Balogun, M. S.; Tong, Y. Co-based MOF-derived Co/CoN/Co_2P ternary composite embedded in N- and P-doped carbon as bifunctional nanocatalysts for efficient overall water splitting. *Int. J. Hydrogen. Energ.* **2019**, *44*, 11402-10. DOI
50. Lu, Y.; Liu, T.; Dong, C. L.; et al. Tailoring competitive adsorption sites by oxygen-vacancy on cobalt oxides to enhance the electrooxidation of biomass. *Adv. Mater.* **2022**, *34*, e2107185. DOI PubMed
51. Li, S.; Wang, S.; Wang, Y.; et al. Doped Mn enhanced NiS electrooxidation performance of HMF into FDCA at industrial-level current density. *Adv. Funct. Mater.* **2023**, *33*, 2214488. DOI
52. Ge, R.; Wang, Y.; Li, Z.; et al. Selective electrooxidation of biomass-derived alcohols to aldehydes in a neutral medium: promoted water dissociation over a nickel-oxide-supported ruthenium single-atom catalyst. *Angew. Chem. Int. Ed. Engl.* **2022**, *61*, e202200211. DOI PubMed
53. Sun, Y.; Wang, J.; Qi, Y.; Li, W.; Wang, C. Efficient electrooxidation of 5-hydroxymethylfurfural using co-doped Ni_3S_2 catalyst: promising for H_2 production under industrial-level current density. *Adv. Sci.* **2022**, *9*, e2200957. DOI PubMed PMC
54. Lu, L.; Wen, C.; Wang, H.; Li, Y.; Wu, J.; Wang, C. Tailoring the electron structure and substrate adsorption energy of Ni hydroxide via Co doping to enhance the electrooxidation of biomass-derived chemicals. *J. Catal.* **2023**, *424*, 1-8. DOI
55. Moysiadou, A.; Lee, S.; Hsu, C. S.; Chen, H. M.; Hu, X. Mechanism of oxygen evolution catalyzed by cobalt oxyhydroxide: cobalt superoxide species as a key intermediate and dioxygen release as a rate-determining step. *J. Am. Chem. Soc.* **2020**, *142*, 11901-14. DOI PubMed
56. Chen, Z.; Cai, L.; Yang, X.; et al. Reversible structural evolution of $NiCoO_xH_y$ during the oxygen evolution reaction and identification of the catalytically active phase. *ACS. Catal.* **2018**, *8*, 1238-47. DOI
57. Li, S.; Sun, X.; Yao, Z.; et al. Biomass valorization via paired electrosynthesis over vanadium nitride-based electrocatalysts. *Adv. Funct. Mater.* **2019**, *29*, 1904780. DOI
58. Liu, J.; Tao, S. Laser promoting oxygen vacancies generation in alloy via Mo for HMF electrochemical oxidation. *Adv. Sci.* **2023**, *10*, e2302641. DOI PubMed PMC